

---

# VQ-NeRV: A Vector Quantized Neural Representation for Videos

---

Yunjie Xu<sup>1</sup>, Xiang Feng<sup>2</sup>, FeiWei Qin<sup>2</sup>, RuiQuan Ge<sup>2</sup>, Yong Peng<sup>2</sup>, Changmiao Wang<sup>3</sup>  
{xiangfeng, qinfeiwei, gespring, yongpeng}@hdu.edu.cn  
{xuyunjie13, cmwangalbert@gmail.com}

## Abstract

Implicit neural representations (INR) excel in encoding videos within neural networks, showcasing promise in computer vision tasks like video compression and denoising. INR-based approaches reconstruct video frames from content-agnostic embeddings, which hampers their efficacy in video frame regression and restricts their generalization ability for video interpolation. To address these deficiencies, Hybrid Neural Representation for Videos (HNeRV) was introduced with content-adaptive embeddings. Nevertheless, HNeRV’s compression ratios remain relatively low, attributable to an oversight in leveraging the network’s shallow features and inter-frame residual information. In this work, we introduce an advanced U-shaped architecture, Vector Quantized-NeRV (VQ-NeRV), which integrates a novel component—the VQ-NeRV Block. This block incorporates a codebook mechanism to discretize the network’s shallow residual features and inter-frame residual information effectively. This approach proves particularly advantageous in video compression, as it results in smaller size compared to quantized features. Furthermore, we introduce an original codebook optimization technique, termed shallow codebook optimization, designed to refine the utility and efficiency of the codebook. The experimental evaluations indicate that VQ-NeRV outperforms HNeRV on video regression tasks, delivering superior reconstruction quality (with an increase of 1-2 dB in Peak Signal-to-Noise Ratio (PSNR)), better bit per pixel (bpp) efficiency, and improved video inpainting outcomes. Code and supplementary materials are available at the link: <https://github.com/magicffourier/VQ-NeRV>.

## 1 Introduction

Given the substantial daily generation of video content, the efficient storage and transmission of these videos are critical tasks in the domains of computer vision and video processing. Despite advancements in modern storage systems, the space required for raw video data remains a formidable challenge. Despite the decrease in storage costs, network speed and I/O processing continue to pose bottlenecks. The vast size of video files contributes to high expenses in both transmission and processing. Traditional video codecs, such as H.264 [28] and HEVC [25], rely on manually-designed encoders and decoders based on the discrete cosine transform [2]. With the success of deep learning, numerous attempts [1, 7] have been made to use neural networks to replace certain components in existing compression frameworks. While these deep learning-based compression methods demonstrate significant potential in terms of rate-distortion, they not only require complex frameworks but also suffer from expensive computational costs during training, encoding, and decoding.

To address the complexity of frameworks and the heavy computational burden, implicit neural representations have gained popularity for their simplicity, usability, and efficiency, such as NeRV [4] for video compression. By representing videos using the hidden-layer features of a neural network,

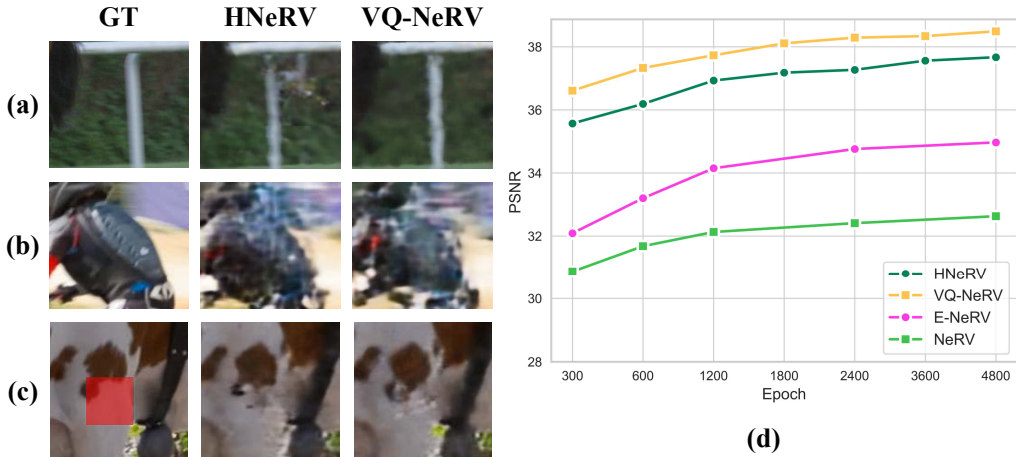


Figure 1: (a) and (b) Video interpolation qualitative results on the DAVIS dataset. (c) Video inpainting qualitative results on the DAVIS dataset. (d) Video regression for hybrid and implicit neural representations with 1.5M parameters on the Bunny dataset.

the video compression problem can be transformed into a model compression problem, which significantly simplifies the encoding and decoding processes and consequently leads to a reduction in computational costs. NeRV’s compression ratio is relatively low due to content-agnostic embeddings, no visual priors, and imbalanced model parameter distribution. Chen et al. [5] proposed a hybrid neural representation approach, HNeRV, employing a VAE-shaped deep network to address these concerns. Despite these efforts, HNeRV continues to suffer from information loss, primarily due to an oversight in harnessing the network’s shallow features. In our work, we introduce an advanced U-shaped architecture, Vector Quantized-NeRV (VQ-NeRV), which integrates a novel component—the VQ-NeRV Block. This component is designed to capture the network’s shallow features, mimicking the functionality of skip connections to truncate the backpropagation "path" [22]. This architectural enhancement contributes to enhanced image reconstruction quality and improved performance in video compression. During the decoding process, to minimize the size of the transmitted bitstream, the encoder is typically excluded from the final bitstream. To tackle this challenge, VQ-VAE [26] discretizes continuous latent embeddings, creating a finite-sized codebook. VQ-NeRV extends the VAE-shaped framework by introducing a VQ-NeRV Block to discretize shallow features from the encoder into a finite-sized codebook. After model training (i.e., encoding), during decoding, skip connections from the encoder are simulated using codebook tokens, thereby further enhancing the network’s ability to reconstruct the given video. To improve codebook utilization and avoid the index collapse problem during training, we propose a reinitialization strategy, termed shallow codebook optimization, designed to refine codebook utility and efficiency, as detailed in Section 3.2. Experimental results demonstrate that even with a small number of codebook tokens, the reconstruction capability of the decoder’s parameters is significantly enhanced. The main contributions of our work are summarized as follows:

- We introduce a novel plug-and-play component called the VQ-NeRV Block. This block discretizes shallow features and inter-frame residual information, thereby enhancing the network’s reconstruction capability and improving video compression performance. During the decoding phase, employing a discretized codebook alongside codebook tokens, the VQ-NeRV Block can simulate skip connections linking the encoder and decoder.
- The VQ-NeRV Block leverages the Haar transform and an invertible block for reversible downsampling and upsampling, effectively mitigating information loss attributed to conventional downsampling modules commonly employed in U-shaped networks.
- Addressing the issue of low usage of code vector nodes due to index collapse in a codebook, we propose a reinitialization strategy, termed shallow codebook optimization, designed to refine codebook utility and efficiency.

## 2 Related Work

### 2.1 Neural Representation

Implicit neural representations fit each independent signal where the neural network is regressed to a specific image, scene, or video. Most implicit neural representations are pixel coordinate-based. These coordinate-based implicit representations find widespread applications in diverse domains, including image reconstruction [24], shape regression [20], and 3D view synthesis [6]. Chen et al. [4] proposed an image-based implicit representation method, taking frame index  $t$  as input and leveraging the neural network’s implicit representation for rapid and accurate image reconstruction, applied to downstream tasks for fast and accurate video compression. Compared to methods relying on pixel coordinates, approaches that depend solely on indices rather than coordinates can expedite the encoding and decoding processes. Subsequent works on implicit representation methods, such as E-NeRV [13], and DNeRV [31], have further improved video regression performance. While implicit neural representations have achieved tremendous success, the absence of content-adaptive embeddings hinders regression capacity.

### 2.2 Video Compression

Traditional video compression methods, such as H.264 [28], and HEVC [25], suffer from the complexity of frameworks and heavy computational burden. In recent years, as deep learning techniques have been increasingly applied to video compression, a series of related works have been proposed. Some fundamentally restructure conventional video compression frameworks employing deep learning tools [1, 17]. Others focus on fine-tuning traditional codec frameworks [9] and optimizing compression frameworks [21]. Some approaches [14, 29] narrow down the problem to image compression and interpolation. NeRV reformulates the entire compression pipeline to achieve video compression, transforming a specific video compression problem into a model compression problem. However, NeRV encounters limitations in regression capacity attributed to the absence of content-adaptive embeddings. In contrast, HNeRV [5] achieved success by forsaking the position embedding function and effectively utilizing content-adaptive latent information. Nevertheless, it still overlooks shallow network feature and inter-frame residual information. In contrast, we use a U-shaped network as our base neural network to propose that VQ-NeRV makes full use of shallow network feature and inter-frame residual information. VQ-NeRV employs a plug-and-play VQ-NeRV Block that uses a codebook mechanism to simulate the functionality of skip connection to connect encoder and decoder. To improve the usage of code vectors, we adopt a code vector nodes expired strategy, contemplating the reset of low-usage code vector nodes during the training process.

### 2.3 Invertible Neural Network

Invertible networks are designed to transform one distribution into another through a bijective function, thereby preserving all information [15]. By utilizing invertible networks, a complex distribution of feature map instances, denoted as  $x \sim p_x(x)$ , can be generated from a given latent variable  $z$ , which follows a simpler distribution  $p_z(z)$ . This transformation is expressed as  $x = f(z)$ , where  $f$  represents the bijective function learned by the network. We employ invertible blocks for downsampling to effectively reduce the decoder size without sacrificing information integrity.

## 3 Pipeline

Firstly we will present an in-depth overview of the proposed VQ-NeRV in Section 3.1. Following this, Section 3.2 will introduce the VQ-NeRV Block, delineating its intricate details. Subsequently, in Section 3.3, we will introduce the shallow codebook optimization. Moreover, in Section 3.4, we will revisit the discussion on loss functions. Finally, in Section 3.5, we will elucidate the methodology for calculating the final bitstream size.

### 3.1 Overview of VQ-NeRV Network

VAE-shaped framework [5] faces a limitation attributable to an oversight in leveraging the network’s shallow features. A U-shaped network is introduced, incorporating skip connections to fully leverage

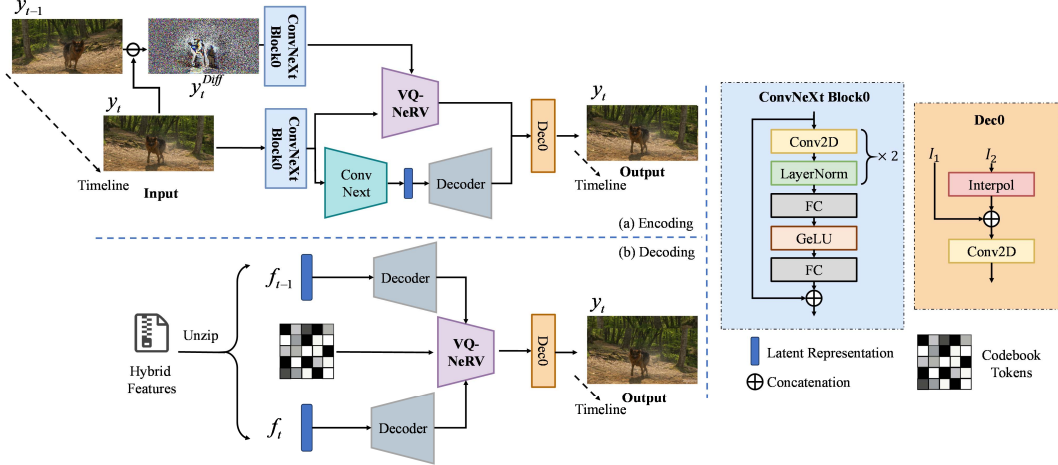


Figure 2: Overview of the proposed method VQ-NeRV. The upper figure is the video encoding processing, and the lower figure is the video decoding processing. In video compression, we train a VAE model for video encoding, utilizing the decoder’s inference processing for the video decoding.

diverse scale features within the network [22]. This inclusion helps mitigate information loss incurred during downsampling. It is widely recognized that larger shallow feature maps contribute to improved reconstruction performance. The codebook mechanism, in contrast to quantized features, leads to a lower bitrate. Furthermore, codebook tokens can be efficiently compressed using entropy compression algorithms. In the VAE-shaped framework [5], the reconstruction performance under high dynamic scene inter-frame residual information is often limited due to the absence of inter-frame information.

To address these shortcomings, as illustrated in the upper part of Fig. 2, we utilize a VQ-NeRV Block module to enhance the decoder’s performance. By integrating a VQ-NeRV Block into the encoder side of the complete U-shaped network, the Block discretizes the shallow residual features and inter-frame residual information during the training process. This discretization is achieved through its embedded codebook mechanism, which contrasts with quant features, resulting in a lower bitrate. During the decoding process, as depicted in the lower part of Fig. 2, VQ-NeRV employs codebook tokens along with context-adaptive embeddings from frame  $t$  and frame  $t - 1$  as inputs. Specifically, it utilizes context-adaptive embeddings from frame  $t - 1$ , combined with half of the codebook tokens, to reconstruct the feature map for frame  $t$ . Simultaneously, it employs context-adaptive embeddings from frame  $t$  along with the remaining codebook tokens to reconstruct the feature map for frame  $t$ . Subsequently, VQ-NeRV fuses these feature maps and feeds them into the decoder to reconstruct the final image. By leveraging both external codebook tokens and the codebook mechanism to simulate skip connections, VQ-NeRV effectively captures the inter-frame residual information as well as the residual information from the encoder to the decoder. This process greatly aids in image reconstruction. Through the concatenation of these shallow residual features, VQ-NeRV significantly enhances its image reconstruction capabilities. Furthermore, the codebook tokens can be easily compressed using entropy compression algorithms.

### 3.2 VQ-NeRV Block Architecture

Due to the imperative of reducing codebook tokens for achieving lower bitrates in video compression tasks, the VQ-NeRV Block needs to downsample the shallow residual feature map and subsequently upsample it for reconstruction, as illustrated in Fig. 3.

In Fig. 2, we illustrate the utilization of feature maps extracted from the initial ConNeXt block of the network [16], obtained from both frame  $t$  and frame  $t - 1$ , in conjunction with the penultimate decoder block, serving as inputs for the VQ-NeRV Block. Here,  $f_e^t$ ,  $f_d^t$ , and  $f_d^{t-1}$  represent the features derived from the encoder at frame  $t$ , the decoder at frame  $t$ , and the decoder at frame  $t - 1$ , respectively. Subsequently, we concatenate  $f_e^t - f_d^t$  and  $f_e^t - f_d^{t-1}$ , which denotes as  $x \in \mathbb{R}^{C_0 \times H_0 \times W_0}$  are then passed into the downsample module. Xiao et al. proposed the wavelet transformation can be used as a reversible downsampling module [30]. As depicted in Fig. 3, the input  $x$  undergoes three

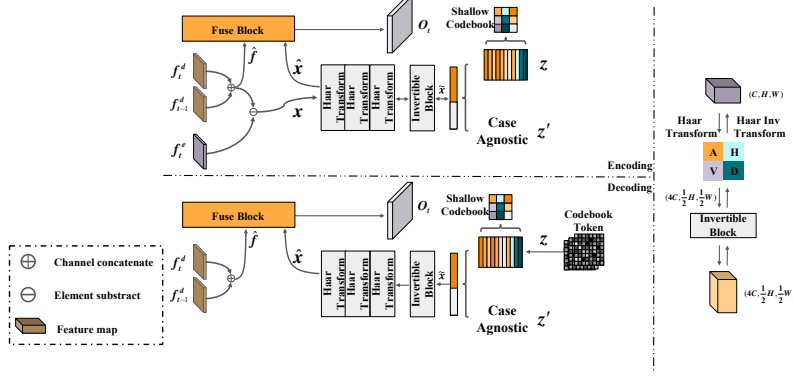


Figure 3: Overview of VQ-NeRV Block Architecture.

down-sampling modules to reduce the dimensions of shallow residual features from  $x \in \mathbb{R}^{C_0 \times H_0 \times W_0}$  to  $x \in \mathbb{R}^{64C_0 \times H_0/8 \times W_0/8}$ . Following this, the VQ-NeRV Block utilizes an invertible block to map  $x \in \mathbb{R}^{64C_0 \times H_0/8 \times W_0/8}$  to the shallow codebook’s discretized residual feature, as well as  $\mathbb{Z}^l$ , which is case agnostic feature. By replacing the original residual feature with the discretized residual feature  $z \in \mathbb{R}^{C_{\text{shallow}} \times H_0/8 \times W_0/8}$ , we obtain  $\tilde{x} \in \mathbb{R}^{64C_0 \times H_0/8 \times W_0/8}$ . Subsequently, we pass  $\tilde{x}$  through the invertible block, followed by the Haar inverse transform, to obtain its upsampled inverse  $\hat{x} \in \mathbb{R}^{C_0 \times H_0 \times W_0}$  and  $\hat{f}$ . The operation of invertible block can be represent as:

$$\begin{aligned}
 v_1 &= x + t_2(f), \\
 v_2 &= f \odot \exp(s_1(v_1)) + t_1(v_1), \\
 \hat{f} &= (v_2 - t_1(v_1)) \odot \exp(-s_1(v_1)), \\
 \hat{x} &= v_1 - t_2(\hat{f}),
 \end{aligned} \tag{1}$$

where  $s_1, s_2, t_1$  and  $t_2$  denote as arbitrary functions. The VQ-NeRV Block fuse  $\hat{x} \in \mathbb{R}^{C_0 \times H_0 \times W_0}$ ,  $f^t$  and  $f^{t-1}$  to the final output layer of the decoder, Dec0 (depicted in Fig. 2). The fuse operation can be represented as:

$$\begin{aligned}
 u_t &= \tanh \left( \text{Conv}(\hat{x}) + \text{Conv}(\hat{f}) \right), \\
 v_t &= \text{Sigmoid} \left( \text{Conv}(\hat{x}) + \text{Conv}(\hat{f}) \right), \\
 O_t &= u_t \odot v_t + (1 - v_t) \odot \hat{x},
 \end{aligned} \tag{2}$$

where  $O_t$  denotes the final output feature maps of frame  $t$ , as depicted in Fig. 3. Consequently, Dec0 is capable of acquiring shallow residual features from the initial ConNeXt block and inter-frame information simultaneously, thereby reducing the parameter count of codebook tokens.

### 3.3 Shallow Codebook Optimization

Given a high-dimensional network feature  $x \in \mathbb{R}^{C_{\text{shallow}} \times H_0/8 \times W_0/8}$ , where  $C_{\text{shallow}}$  is equal to  $64C_0$ . The shallow codebook learns  $N$  embedding vectors  $z_{q_i} \in \mathbb{R}^{C_{\text{shallow}} \times 1 \times 1}, i = 0..N$  to embed the image, which  $C_{\text{shallow}}$  represents the dimensionality of the embedded vectors in the codebook. The shallow codebook maps the input continuous network features  $x_i \in \mathbb{R}^{C_{\text{shallow}} \times 1 \times 1}$  by looking up the closest clustered features  $e_k \in \mathbb{R}^{C_{\text{shallow}} \times 1 \times 1}, k = 1..N$  in the codebook  $\mathcal{Z} = \{e_i | i = 1..N\}$ . Finally, the quantized features  $\hat{z} \in \mathbb{R}^{C_{\text{shallow}} \times H_0/8 \times W_0/8}$  are obtained through a codebook mechanism.

However, this codebook mechanism consistently faces challenges associated with low utilization. Practical experiments have revealed that lower utilization of shallow features can adversely hamper

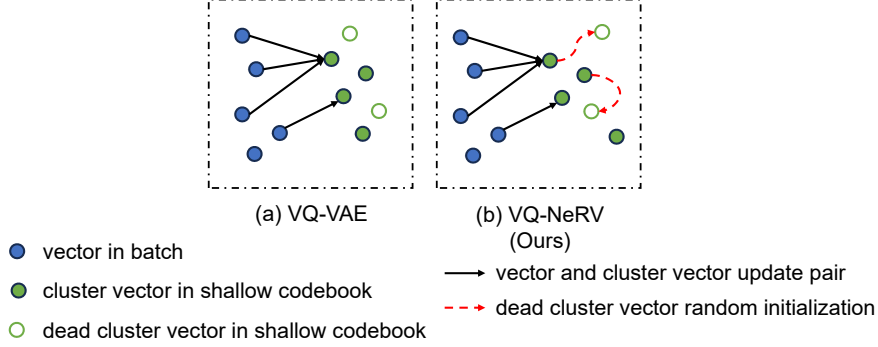


Figure 4: (a) The selection criteria for Exponential Moving Average (EMA) updates within a batch of VQ-VAE. (b) The proposed strategy for optimizing the shallow codebook.

the performance of video regression capabilities. With the high dimensionality involved in the exponential moving average (EMA) update process, it is crucial to appropriately initialize the weights to ensure higher quality image reconstruction. To address this concern, Hu et al. [8] propose a strategy to replace "dead" codes with randomly selected batch features to increase the utilization of the codebook, as depicted in Fig. 4 (a). However, VQ-NeRV adopts a relatively low batch size (batch=1), and randomly sampling batch features with such a low batch size could limit the performance of reconstruction. The quantitative performance comparison is presented in Section 4.6 of the experiments. To mitigate these issues, this paper proposes the following three steps:

- 1) We utilize a feature pool that is the same size as the codebook. Initially, we randomly sample the first several batch features to initialize the original cluster nodes. This feature pool is used to store and cluster the cluster nodes throughout the entire training process.
- 2) During each EMA update step of the codebook, we first utilize the k-means algorithm to obtain the current batch cluster nodes using the cluster nodes from the feature pool. Subsequently, we update the cluster nodes of the feature pool using the EMA update strategy.
- 3) After each EMA update step of the codebook, we select the cluster node  $e_{\text{dead}} \in \mathbb{R}^{C_{\text{shallow}} \times 1 \times 1}$  whose cluster size is smaller than the dead node threshold set by a hyperparameter, excluding the zero vector. For the cluster node  $e_{\text{dead}} \in \mathbb{R}^{C_{\text{shallow}} \times 1 \times 1}$ , we replace it with the closest cluster node in the feature pool whose cluster size exceeds the dead node threshold, as depicted in Fig. 4 (b).

This strategy aims to mitigate the limitations associated with a small batch size and further enhance the video regression capabilities.

### 3.4 Loss Function

During training processing, encoder, decoder, codebook ( $\mathcal{Z}$ ) and the VQ-NeRV Block are jointly optimized, and this optimization process can be represented as:

$$\mathcal{L}_q = \|sg[\varepsilon_\phi(x)] - z_q\|_2^2 + \beta \|\varepsilon_\phi(x) - sg[z_q]\|_2^2, \quad (3)$$

where  $sg[\bullet]$  represents the gradient stop operation, and the first part of Eq. 3 corresponds to the original  $\mathcal{L}_2$  loss,  $\varepsilon_\phi$  denotes the entire encoder and the invertible block within the VQ-NeRV Block,  $\beta$  in Eq. 3 represents the weight of the second part of the loss.

Due to VQ-NeRV aiming to reconstruct high-quality videos, we use the  $\mathcal{L}_1$  loss function and SSIM loss function to optimize the overall reconstruction loss of the VQ-NeRV framework. This can be expressed as:

$$\mathcal{L}_{\text{reconstruct}}(\hat{x}, \tilde{x}) = \alpha \|\hat{x} - \tilde{x}\|_1 + (1 - \alpha)(1 - SSIM(\hat{x}, \tilde{x})), \alpha = 0.7 \quad (4)$$

where  $\hat{x}$  denotes the final reconstruction image,  $\tilde{x}$  denotes the ground truth. For partially distorted video, i.e., video inpainting, we use  $\mathcal{L}_{\text{inpainting}} = (1 - M) \times \mathcal{L}_{\text{reconstruct}}(x, \hat{x})$  as the loss function, where

$M$  is a mask matrix, where distorted pixels are marked as 1, and others are 0. The comprehensive loss for the normal video compression task is represented as  $\mathcal{L}_{total} = \mathcal{L}_{reconstruct} + \mathcal{L}_q$ , whereas for the image inpainting task, it is denoted as  $\mathcal{L}_{total} = \mathcal{L}_{inpainting} + \mathcal{L}_q$ .

### 3.5 Down Task

**Video Compression.** Li et al. [13] propose that embedding and model quantization are identified as crucial elements contributing to a notable reduction in the final model size. Further investigation reveals that the compression of content-adaptive embedding, specifically through entropy coding, yields significant outcomes. Consequently, in our method, we employ the deflate algorithm [19] for both compressing embedding features and codebook tokens. This method achieves a bitrate saving of close to 14% compared to using Huffman coding alone. The total size of VQ-NeRV comprises frame embedding features, whose shape is  $2 \times 16 \times 8$ , along with codebook tokens of  $2 \times 16$  for each frame at a resolution of  $1280 \times 640$ . Additionally, it encompasses decoder parameters, with the caveat that only utilized quant codebook embeddings are transmitted, but not including the transmission of zero vectors. The total size can be expressed as:

$$\begin{aligned} TotalSize = & frameNumbers * (latentEmbedding + codebookToken) \\ & + decoderSize + CodebookEmbedding. \end{aligned} \quad (5)$$

## 4 Experiments

In this section, we will first introduce the dataset and hyperparameter settings used in the experiments in Section 4.1. Secondly, Section 4.2 will depict the main results of video representation. Comparative results for video compression will be presented in Section 4.3, while Section 4.4 will exhibit results for video inpainting and results for video interpolation in Section 4.5. Finally, Section 4.6 will present ablation study results for the VQ-NeRV.

### 4.1 Datasets and Implementation Details

The datasets used include Big Buck Bunny (Bunny) [23], UVG [18], and DAVIS [27]. The Bunny dataset consists of 132 frames with a resolution of  $720 \times 1280$ . The UVG dataset has 7 videos with a size of  $1080 \times 1920$ , with 120 FPS, and a duration of 5s or 2.5s. DAVIS is a high-quality, high-resolution dataset for video object segmentation. For a fair comparison, we follow the settings of [5] and center-crop the videos into  $640 \times 1280/960 \times 1920$  for all experiments.

VQ-NeRV uses the Adam optimizer with betas as (0.9,0.999), weight decay set to 0, and learning rate at 0.001 with cosine learning rate decay. And we also use batch size as 1. For the codebook configuration in VQ-NeRV, the codebook size is set to be larger than the input feature map size, typically choosing 1024/2048 for resolutions  $1280 \times 640/1920 \times 960$ . The codebook dimension is set to 8. The threshold for "dead" code is set to 1. We maintain the stride list for an input/output size of  $1280 \times 640/1920 \times 960$  with strides (5, 4, 4, 2, 2)/(5, 4, 4, 3, 2), and the kernel size and reduction rate remain the same as [5].

In the video interpolation task, we train the model on the sequence of even frames and test it on the odd frames sequence from the UVG and the DAVIS dataset. And in the video inpainting task, we directly use the models trained in regression without any fine-tuning and test them using masked videos in disperse mask from the UVG and the DAVIS dataset.

### 4.2 Video Regression

In this section, we compare the performance of VQ-NeRV with other state-of-the-art implicit methods on the Bunny dataset [23], as well as the state-of-the-art hybrid implicit-based method. Table 1 shows the results of the video regression performance under the same size and 300 epochs. The results demonstrate that the VQ-NeRV significantly surpasses that of the hybrid neural representation method HNeRV on the Bunny dataset on video regression reconstruction performance. Fig. 1 (a) and Table 1 show comparison results under the same sizes (0.75M and 1.5M) and different training times. The results indicate that VQ-NeRV converges faster compared to hybrid neural representation methods such as HNeRV and DNeRV.



Figure 5: Visualization comparing VQ-NeRV with other state-of-the-art methods for several patches on the 131st frame of the Bunny Dataset at the same extremely low size of the decoder (0.35M), corresponding to 0.0182 bpp of our VQ-NeRV.

Table 1: Video regression with varying sizes and different epochs with 0.75M decoder size on the Bunny dataset, PSNR $\uparrow$  reported.

Method	Size				Epoch					
	0.35M	0.75M	1.5M	3M	300	600	1,200	1,800	2,400	3,600
NeRV [4]	26.99	28.46	30.87	33.21	28.46	29.15	29.57	29.73	29.77	29.86
E-NeRV [13]	27.84	30.95	32.09	36.72	30.90	32.07	32.79	33.10	33.36	33.67
HNeRV [5]	30.15	32.81	35.57	37.43	32.81	33.89	34.51	34.71	34.88	35.03
DNeRV [31]	30.80	33.30	35.22	38.09	33.30	34.28	34.83	35.16	35.25	35.34
<b>VQ-NeRV(Ours)</b>	<b>31.06</b>	<b>34.00</b>	<b>36.61</b>	<b>39.05</b>	<b>33.61</b>	<b>35.68</b>	<b>35.57</b>	<b>35.76</b>	<b>35.91</b>	<b>36.15</b>

Table 2: Video regression at resolution 960 $\times$ 1920 on the UVG dataset, PSNR $\uparrow$  reported.

Method	Beauty	Bospho	Honey	Jockey	Ready	shake	yach	Avg
NeRV [4]	33.25	33.22	37.25	31.74	24.84	33.08	28.03	31.63
E-NeRV [13]	33.17	33.69	37.63	31.63	25.24	34.39	28.42	32.02
HNeRV [5]	33.58	34.73	38.96	32.04	25.74	34.57	29.26	32.69
PS-NeRV [3]	32.94	32.32	38.39	30.38	23.61	33.26	26.33	31.13
DNeRV [31]	33.91	33.17	38.22	32.01	25.56	33.58	27.15	31.94
FFNeRV [11]	33.57	35.03	38.95	31.57	25.92	34.41	28.99	32.63
HiNeRV [10]	34.08	36.57	<b>39.71</b>	36.10	31.53	35.85	30.95	34.97
<b>VQ-NeRV(Ours)</b>	<b>34.15</b>	<b>36.89</b>	39.41	<b>36.77</b>	<b>31.74</b>	<b>36.08</b>	<b>32.85</b>	<b>35.41</b>

Fig. 5 also depicts a detailed comparison of the image reconstruction performance between VQ-NeRV and other state-of-the-art methods at an extremely low decoder size (0.35M). Note that we have reconfigured position-embedding based methods to operate at an extremely low size. However, we find that DNeRV [31] cannot operate effectively at that decoder size on the Bunny dataset. FFNeRV also faces similar issues, although it performs slightly better than DNeRV. For the remaining state-of-the-art methods, at extremely low bpp, VQ-NeRV exhibits better reconstruction details than others, as depicted in Fig. 5. We note that the bounding box labeled as 1 highlights the position where other methods even generated incorrect patches. To cover a broader range of sequences, we also conduct reconstruction performance on the UVG dataset. We maintain the size of all position-embedding based methods limited to 3M, and we also limit the size of hybrid neural representation methods and their content-adaptive embeddings to 3M. Through the incorporation of shallow residual features, VQ-NeRV surpasses HNeRV and achieves comparable results with other state-of-the-art methods.



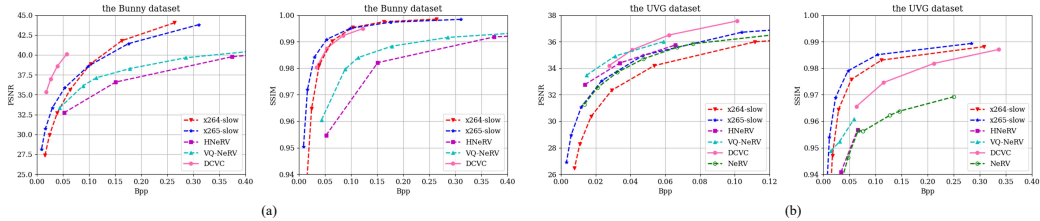


Figure 6: (a) Compression results on the bunny dataset. (b) Compression results on the UVG dataset.

Table 3: Video Inpainting results (PSNR $\uparrow$ ) with 5 fixed box masks on input videos on the DAVIS dataset. ‘Input’ is the baseline of mask video and ground truth.

Method	bike	b-swan	bmxb	b-danccamelc	rounc-shado	cows	d-twirl	dog	Avg		
Input	23.14	20.24	19.99	21.36	17.3	20.47	18.92	19.37	20.45	18.39	19.96
HNeRV [5]	28.37	29.49	29.77	27.86	27.4	26.94	29.96	24.15	27.89	30.72	28.26
<b>VQ-NeRV(Ours)</b>	<b>31.74</b>	<b>32.26</b>	<b>33.22</b>	<b>31.12</b>	<b>27.4</b>	<b>28.53</b>	<b>33.57</b>	<b>24.89</b>	<b>28.26</b>	<b>33.38</b>	<b>30.44</b>

Table 4: Video interpolation results at resolution 960 $\times$ 920 on the UVG and DAVIS dataset, PSNR $\uparrow$  reported. ‘Input’ is the baseline of mask video and ground truth.

Method	beauty	b-swan	bmxb	b-danccamel	bee	jockey	ready	shake	yach	Avg	
NeRV [4]	28.05	17.94	15.55	16.99	14.83	36.99	20.00	17.02	29.15	24.50	22.10
HNeRV [5]	31.10	<b>21.44</b>	18.29	20.29	20.64	38.83	23.82	20.99	32.61	<b>27.24</b>	25.52
<b>VQ-NeRV(Ours)</b>	<b>31.15</b>	21.08	<b>19.33</b>	<b>20.63</b>	<b>20.64</b>	<b>38.98</b>	<b>24.33</b>	<b>21.18</b>	<b>32.75</b>	27.15	<b>25.72</b>

### 4.3 Video Compression

With global L1 norm pruning (10%), embedding quantization (8-bit), model quantization (8-bit), embedding and model entropy coding (8% saved), and deflate (7% saved) of codebook tokens, the results of model compression on the UVG and bunny dataset, as shown in Fig. 6. For the Bunny dataset, as depicted in Fig. 6(a), VQ-NeRV surpasses HNeRV but falls short of other methods, mainly due to the inherent performance characteristics of the HNeRV block. However, in Fig. 6(b), VQ-NeRV demonstrates superior compression performance compared to implicit neural-based methods such as HNeRV, NeRV, and DCVC [12], as well as traditional video codecs x264 preset-slow and x265 preset-slow on the UVG dataset. VQ-NeRV not only consistently enhances performance when the camera is stationary, but also improves performance in highly dynamic scenes due to the utilization of inter-frame residual information. Actual experiments demonstrate that the more inter-frame residual information is involved, the better the reconstruction performance. Due to the balance of bitrate, we only utilize frame  $t - 1$  to aid in reconstructing frame  $t$ .

### 4.4 Video Inpainting

In this section, we also explore the method of using a fixed mask for video inpainting. For the fixed mask, we follow the settings of [5], using 5 boxes of width 50. Given that HNeRV did not publicly release testing scripts for the DAVIS dataset, we re-evaluated the video inpainting performance of HNeRV on the DAVIS dataset. We set the model size to 1.5M, cropped the images to 960  $\times$  920, and set the stride list to (5,4,4,3,2). We have rerun their experiment on the DAVIS dataset. Table 3 displays the quantitative results between VQ-NeRV and HNeRV on different sequences, showing that VQ-NeRV outperforms HNeRV in image inpainting performance.

### 4.5 Video Interpolation

Given that the INR-based video representation tends to overfit the given video, we evaluate the generalization capabilities of various methods by video interpolation tasks. Following the settings of [5], we train the model on the sequence of even frames and test it on the odd frames sequence on the UVG and DAVIS dataset and present the quantitative results of the UVG dataset in Table 4.

Table 5: Ablation study of different codebook settings on the Bunny dataset in PSNR $\uparrow$  and codebook usage $\uparrow$  in VQ-NeRV Block.

Method	PSNR $\uparrow$	Usage $\uparrow$
baseline	35.52	-
+VQ-NeRV Block	36.25	39.26%
+Shallow Codebook Optimization	36.60	100%
codebook_dim=2	36.20	37.70%
codebook_dim=4	36.54	37.70%
codebook_dim=64	36.61	37.70%
use_cosine	35.82	26.37%
codebook_size=128	36.19	88.28%
codebook_size=256	36.58	64.45%
codebook_size=1,024	36.60	22.27%

Table 4 demonstrates that the generalization capability of video interpolation for INR-based methods is quite challenging. As shown in Table 4, VQ-NeRV exhibits a comparable performance compared to HNeRV, even achieving up to a 5% enhancement, particularly in sequences with significant motion, such as bmx.

#### 4.6 Ablation Study

**Contribution of VQ-NeRV Block and Shallow Codebook Optimization.** In this section, we first compare the performance between the HNeRV and the VQ-NeRV. Secondly, we explore the influence of the Shallow Codebook Optimization proposed in Section 3.2. The experimental results are presented in Table 5. As depicted in Table 5, the proposed VQ-NeRV Block improves +0.73 PSNR on the Bunny dataset, demonstrating the enhanced image reconstruction performance achieved through the simulated skip connection introduced by the VQ-NeRV Block. Additionally, Table 5 shows that with the shallow codebook optimization strategy, the reconstruction performance is further improved, approaching an increase of +0.3 PSNR.

**Contribution of Different Codebook Settings.** In this section, we also explore the comparison of PSNR and codebook usage under different settings of VQ-NeRV Block’s codebook. The results are presented in Table 5. Table 5 shows that using the Euclidean distance yields better codebook usage for the VQ-NeRV Block compared to cosine distance. As depicted in Table 5, we compare different dimensions of the codebook, showing that a larger codebook dimension generally results in better performance. However, considering the impact of codebook size on video compression, we opt for a compromise and choose codebook\_dim = 8. According to the ablation study settings in Table 5, the size of the feature map of the initial ConNeXt block is 256. Comparing different codebook sizes, Table 5 shows that smaller codebook sizes result in higher codebook usage. However, performance tends to decline when the codebook size is lower than the size of the feature map of the initial ConNeXt block. Therefore, considering a trade-off between codebook size and performance, we select codebook\_size = 512 for a resolution of  $1280 \times 640$ .

## 5 Conclusion

In this paper, we propose an enhanced network, VQ-NeRV, which applies a U-Net shape network to learn vector quantized neural representations using a codebook mechanism. The VQ-NeRV Block, through the utilization of the codebook mechanism, discretizes the network’s shallow residual features and inter-frame information. During decoding processing, the codebook tokens are employed to simulate the skip connections function. Compared to HNeRV, VQ-NeRV reduces network depth by skip connections and integration of inter-frame information, leading to an enhanced compression ratio while maintaining the same reconstruction quality and faster convergence speed at an equivalent size. As a video representation method, VQ-NeRV Block can be seamlessly integrated into HNeRV, providing advantages in terms of reconstruction performance and compression ratio with a judiciously designed size. Nevertheless, VQ-NeRV does have certain limitations. As an implicit representation-based method, it necessitates training processing to adapt to new videos, and it requires hyperparameter

adjustment to achieve optimal performance. In our future work, we aim to explore methods for determining suitable encoding parameters to achieve an optimal compression ratio, particularly tailored for different decoder sizes, even when applied to previously unseen videos.

## References

- [1] E. Agustsson, D. Minnen, N. Johnston, J. Balle, S. J. Hwang, and G. Toderici. Scale-space flow for end-to-end optimized video compression. In *CVPR*, pages 8503–8512, 2020.
- [2] N. Ahmed, T. Natarajan, and K. R. Rao. Discrete cosine transform. *TC*, 100(1):90–93, 1974.
- [3] Y. Bai, C. Dong, C. Wang, and C. Yuan. Ps-nerv: Patch-wise stylized neural representations for videos. In *ICIP*, pages 41–45. IEEE, 2023.
- [4] H. Chen, B. He, H. Wang, Y. Ren, S. N. Lim, and A. Shrivastava. Nerv: Neural representations for videos. *NeurIPS*, 34:21557–21568, 2021.
- [5] H. Chen, M. Gwilliam, S.-N. Lim, and A. Shrivastava. Hnerv: A hybrid neural representation for videos. In *ICCV*, pages 10270–10279, 2023.
- [6] X. Feng, Y. He, Y. Wang, C. Wang, Z. Kuang, J. Ding, F. Qin, J. Yu, and J. Fan. Zs-srt: An efficient zero-shot super-resolution training method for neural radiance fields. *arXiv preprint arXiv:2312.12122*, 2023.
- [7] A. Habibian, T. v. Rozendaal, J. M. Tomczak, and T. S. Cohen. Video compression with rate-distortion autoencoders. In *ICCV*, pages 7033–7042, 2019.
- [8] M. Huh, B. Cheung, P. Agrawal, and P. Isola. Straightening out the straight-through estimator: Overcoming optimization challenges in vector quantized networks. *arXiv preprint arXiv:2305.08842*, 2023.
- [9] M. Khani, V. Sivaraman, and M. Alizadeh. Efficient video compression via content-adaptive super-resolution. In *ICCV*, pages 4521–4530, 2021.
- [10] H. M. Kwan, G. Gao, F. Zhang, A. Gower, and D. Bull. Hinerv: Video compression with hierarchical encoding-based neural representation. *NeurIPS*, 36, 2024.
- [11] J. C. Lee, D. Rho, J. H. Ko, and E. Park. Ffnerv: Flow-guided frame-wise neural representations for videos. In *ACMMM*, pages 7859–7870, 2023.
- [12] J. Li, B. Li, and Y. Lu. Deep contextual video compression. *NeurIPS*, 34:18114–18125, 2021.
- [13] Z. Li, M. Wang, H. Pi, K. Xu, J. Mei, and Y. Liu. E-nerv: Expedite neural video representation with disentangled spatial-temporal context. In *ECCV*, pages 267–284. Springer, 2022.
- [14] J. Liu, S. Wang, W.-C. Ma, M. Shah, R. Hu, P. Dhawan, and R. Urtasun. Conditional entropy coding for efficient video compression. In *ECCV*, pages 453–468. Springer, 2020.
- [15] Y. Liu, Z. Qin, S. Anwar, S. Caldwell, and T. Gedeon. Are deep neural architectures losing information? invertibility is indispensable. In *ICONIP*, pages 172–184. Springer, 2020.
- [16] Z. Liu, H. Mao, C.-Y. Wu, C. Feichtenhofer, T. Darrell, and S. Xie. A convnet for the 2020s. In *CVPR*, pages 11976–11986, 2022.
- [17] G. Lu, W. Ouyang, D. Xu, X. Zhang, C. Cai, and Z. Gao. Dvc: An end-to-end deep video compression framework. In *CVPR*, pages 11006–11015, 2019.
- [18] A. Mercat, M. Viitanen, and J. Vanne. Uvg dataset: 50/120fps 4k sequences for video codec analysis and development. In *ACMMM*, pages 297–302, 2020.
- [19] S. Oswal, A. Singh, and K. Kumari. Deflate compression algorithm. *International Journal of Engineering Research and General Science*, 4(1):430–436, 2016.
- [20] J. J. Park, P. Florence, J. Straub, R. Newcombe, and S. Lovegrove. DeepSDF: Learning continuous signed distance functions for shape representation. In *CVPR*, pages 165–174, 2019.
- [21] O. Rippel, A. G. Anderson, K. Tatwawadi, S. Nair, C. Lytle, and L. Bourdev. Elf-vc: Efficient learned flexible-rate video coding. In *CVPR*, pages 14479–14488, 2021.
- [22] O. Ronneberger, P. Fischer, and T. Brox. U-net: Convolutional networks for biomedical image segmentation. In *MICCAI*, pages 234–241. Springer, 2015.
- [23] T. Roosendaal. Big buck bunny. In *SIGGRAPH*, pages 62–62. 2008.

- [24] V. Sitzmann, J. Martel, A. Bergman, D. Lindell, and G. Wetzstein. Implicit neural representations with periodic activation functions. *NeurIPS*, 33:7462–7473, 2020.
- [25] G. J. Sullivan, J.-R. Ohm, W.-J. Han, and T. Wiegand. Overview of the high efficiency video coding (hevc) standard. *TCSVT*, 22(12):1649–1668, 2012.
- [26] A. Van Den Oord, O. Vinyals, et al. Neural discrete representation learning. *NeurIPS*, 30, 2017.
- [27] H. Wang, W. Gan, S. Hu, J. Y. Lin, L. Jin, L. Song, P. Wang, I. Katsavounidis, A. Aaron, and C.-C. J. Kuo. Mcl-jcv: a jnd-based h. 264/avc video quality assessment dataset. In *ICIP*, pages 1509–1513. IEEE, 2016.
- [28] T. Wiegand, G. J. Sullivan, G. Bjontegaard, and A. Luthra. Overview of the h. 264/avc video coding standard. *IEEE TIP*, 13(7):560–576, 2003.
- [29] C.-Y. Wu, N. Singhal, and P. Krahenbuhl. Video compression through image interpolation. In *ECCV*, pages 416–431, 2018.
- [30] M. Xiao, S. Zheng, C. Liu, Y. Wang, D. He, G. Ke, J. Bian, Z. Lin, and T.-Y. Liu. Invertible image rescaling. In *ECCV*, pages 126–144. Springer, 2020.
- [31] Q. Zhao, M. S. Asif, and Z. Ma. Dnerv: Modeling inherent dynamics via difference neural representation for videos. In *CVPR*, pages 2031–2040, 2023.